Climate Dynamics (2020) 54:1655–1669
https://doi.org/10.1007/s00382-019-05079-3

Variability of boreal spring Hadley circulation over the Asian monsoon domain and its relationship with tropical SST

Yaqi Wang[1] · Juan Feng[1] · Jianping Li[2] · Ran An[1] · Lanning Wang[1]

Received: 1 August 2019 / Accepted: 4 December 2019 / Published online: 10 December 2019

Abstract
The variability of boreal spring Hadley circulation (HC) over the Asian monsoon domain over the last four decades is explored. The climatological distribution of the regional HC is symmetric of the equator, with the ascending branch around the equator and sinking branch around the subtropics in each hemisphere. The first dominant mode (EOF1) of the regional HC is equatorial asymmetric, with the main body in the Southern Hemisphere (SH) and the ascending branch to the north of the equator. This mode is mainly characterized by interannual variation and is related to El Niño-Southern Oscillation (ENSO). Significant negative sea surface temperature (SST) anomalies are observed over the tropical Indian Ocean (TIO) along with the development of La Niña events; however, the magnitude of SST anomalies in the southern Indian Ocean is greater than that in the northern counterpart, contributing to EOF1 formation. The spatial distribution of the second dominant mode (EOF2) is with the main body lying in the Northern Hemisphere (NH) and the ascending branch located to the south of the equator. The temporal variation of this mode is connected to the warming of the TIO. The warming rate of the southern TIO SST is faster than that in the northern counterpart, resulting in the southward migration of the rising branch. The above result indicates the critical role of the meridional distribution of SST on the variability of the regional HC.

Keywords Hadley circulation · La Niña events · Tropical Indian Ocean · Sea surface temperature

1 Introduction

Hadley circulation (HC) was first proposed by Hadley (1735) to describe the zonal mean vertical circulation that rises near the equator and sinks in the subtropical zone due to the uneven heating of the sun. The HC is a conveyor belt connecting low latitudes of the equatorial and subtropical regions, and it is also an important factor in global atmospheric circulation changes (Hou 1998; Huang et al. 2019). The HC connects the tropical and extratropical belts, and its ascending and descending branches are usually closely related to precipitation (Numaguti 1995). The HC can transport angular momentum, water vapor, and energy to extratropical regions, thus having an important effect on extratropical and tropical climate anomalies (Trenberth and Stepaniak 2003).

Because the HC is a direct thermodynamic circulation, the sea surface temperature (SST) variations have important impacts on the HC's variation. Early theoretical studies have shown that the meridional structure of the underlying SST affects the location of the ascending and subsidence branches of the HC (Rind and Rossow 1984). The meridional structure of SST can influence the location and intensity of convergence rise by adjusting the convergence process of the boundary layer of atmosphere and the thermodynamic structure (Schneider and Lindzen 1977; Feng and Li 2013). The numerical result also shows that the convergence and divergence of the lower atmosphere are sensitive to the heating location and the longitudinal distribution of the heating profile (Hou and Lindzen 1992). Therefore, the variation in tropical SST has an important influence on the HC. As the strongest factor in the interannual variability in tropical air-sea interaction, El Niño-Southern Oscillation (ENSO) plays an essential role in the HC variations. A previous study found that the HC would significantly strengthen when warmer SST anomalies (SSTA) occurred over the

✉ Juan Feng
fengjuan@bnu.edu.cn

[1] College of Global Change and Earth System Science (GCESS), Beijing Normal University, Beijing 100875, China

[2] Key Laboratory of Physical Oceanography, Institute for Advanced Ocean Studies, Qingdao National Laboratory for Marine Science and Technology, Ocean University of China, Qingdao 266100, China

eastern equatorial Pacific (Oort and Yienger 1996). This is because the warm ENSO events can warm the tropical area and intensify the subtropical jet, which in turn strengthens the HC (Seager et al. 2003). When ENSO is in a neutral or cold phase, the HC intensity is much weaker than that during warm events (Stachnik and Schumacher 2011). Meanwhile, the relationship between the boreal winter HC and El Niño was considered (Mitas and Clement 2006; Stachnik and Schumacher 2011). The impacts of El Niño on the HC are different between the developmental and decay phases (Sun and Zhou 2014). In addition, it is reported that the influences of El Niño on the HC exert significant regional differences, e.g., Wang (2004, 2005) found that during the warm phase of ENSO, the western Pacific HC and Atlantic HC are weakened, whereas the eastern Pacific HC is strengthened. Additionally, it has been reported that the occurrence of ENSO events is related to equatorially symmetric meridional circulation anomalies (Feng and Li 2013; Feng et al. 2019). The different responses of the HC to SST during ENSO events has been verified by models, given that El Niño and La Niña are the most significant interannual signals in the tropical air-sea system (Chen et al. 2016, 2017). In addition, it is found that the variation of SST over the tropical Indian Ocean and western Pacific contributes significantly to the long-term variation of the HC. The long-term warming of SST over this region is considered to be an important factor in modulating the long-term variability of the seasonal HC (Quan et al. 2004; Feng and Li 2013; Guo et al. 2016). The above work indicates that the tropical SST plays an important role in the HC variation.

Although much attention has been paid to the variation of the global HC, the regional characteristics of the HC have also been studied. Because the ascending and descending branches of the HC are well related to convection, the variability of regional HC may have important implications for regional climate change (Chen et al. 2014a; Zhang and Wang 2013; Zhang et al. 2015). Therefore, it is of great significance to study regional HC. Chen et al. (2014b) attempted to detect the HC intensity trend by separating the tropical zonal belt into six regions. Guo and Tan (2018) found that the strength of the regional HC over the Indo-Pacific warm pool area during boreal spring has a significant impact on the tropical cyclone activity over the western North Pacific in the following summer and subsequently influenced the regional rainfall. It was also found that there are strong differences in the regional HC in terms of both intensity and impacts (Nguyen et al. 2015, 2017). For example, some studies have shown that when El Niño occurs, the intensity of HC in the Indian Ocean and South America is abnormally low (Freitas and Ambrizzi 2015; Freitas et al. 2017), while the HC in the eastern Pacific is abnormally strong (Wang 2002; Zeng et al. 2011; Huang et al. 2018a, b). The anomalous changes of HC in these regions have a significant impact on regional climate change. There is substantial evidence that changes of the HC are responsible for the increase of droughts in extratropical regions, such as southern Australia (Fyfe et al. 2012), Altiplano in South America (RenéD and Patricio 2001), South Africa, and Southeast Asia (Dai 2013). Meanwhile, the intensity, boundary, and circulation characteristics of the regional HC are also concerned (Fu et al. 2006; Nguyen et al. 2013). The cross-equatorial cell of the HC shows a significant interdecadal weakening in the tropical monsoon region of the Eastern Hemisphere, which may be the reason for the weakening of tropical monsoons in the South China Sea monsoon region and the East South Asian monsoon region (Wang 2001a; Zhou 2008).

The above discussion shows that the variations of regional HC have obvious regional characteristics. However, most of the studies regarding the regional HC were concentrated on the characteristics of the HC itself and little attention has been given to its variability, especially the dominant mode characteristics. The variability of circulation over the Asian monsoon domain has been extensively studied, as it occurs in the region with the strongest convective activity, the largest latent heat release, the largest moisture content, and the largest interannual variability in the world (Li and Michio 1996; Wang 2001b). As mentioned above, variations of SST over the tropical Indian Ocean (TIO) have an important impact on the global HC; however, their potential impacts on regional HC remain unknown. Meanwhile, it has been reported that the TIO SST variations are also affected by ENSO events (Schott et al. 2008). Therefore, whether ENSO has a potential effect on the variation of this regional HC is undetermined. Additionally, the difference between the influences of the ENSO and TIO SSTs on the HC in this region and the possible cause of this difference remains unknown. Considering that the greatest influence of ENSO on the TIO SST occurs during the boreal spring of its recession period, this paper will focus on this season to investigate the long-term variability characteristics of the HC in the Asian monsoon domain and to illustrate the characteristics of its variability, as well as the possible causes. The organization of this paper is as followed: In Sect. 2, the datasets, methodology and model are described. The variability of the boreal spring HC over the Asian monsoon domain is shown in Sect. 3. In Sect. 4, the role of tropical SST in influencing the regional HC is described. We verify the conclusions with Gill's model in Sect. 5. Finally, our conclusions and discussion are presented in Sect. 6.

2 Datasets, methodology and model

2.1 Datasets

The monthly averaged circulation datasets and two global SST reanalysis datasets we used in this study are described

in Table 1. The Niño 3 index is used to identify the ENSO events (areal averaged SST over 5° S–5° N, 150° W–90° W) available via https://www.esrl.noaa.gov/psd/gcos_wgsp/Timeseries/Data/nino3.long.anom.data. The selection of La Niña events was based on the monthly Niño 3 index that was below −0.5 °C for at least 9 months. We selected 6 La Niña events: 1984/1985, 1988/1989, 1998/1999, 1999/2000, 2007/2008, and 2010/2011. These events are consistent with previous studies (Hoell et al. 2014; Zhang et al. 2015).

Table 1 Datasets used in this study

Abbreviation	Organization	Resolution (lon × lat)	References
HadISST	UK Met Office Hadley Centre's sea ice and SST dataset	1° × 1°	Rayner et al. (2003)
ERSST	Extended Reconstructed SST version 3	2° × 2°	Smith et al. (2008)
NCEP/NCAR	National Center for Environmental Prediction/National Center Atmospheric Research	2.5° × 2.5°	Kalnay et al. (1996)
JRA	Japanese 55-year Reanalysis dataset	1.25° × 1.25°	Kobayashi et al. (2015)

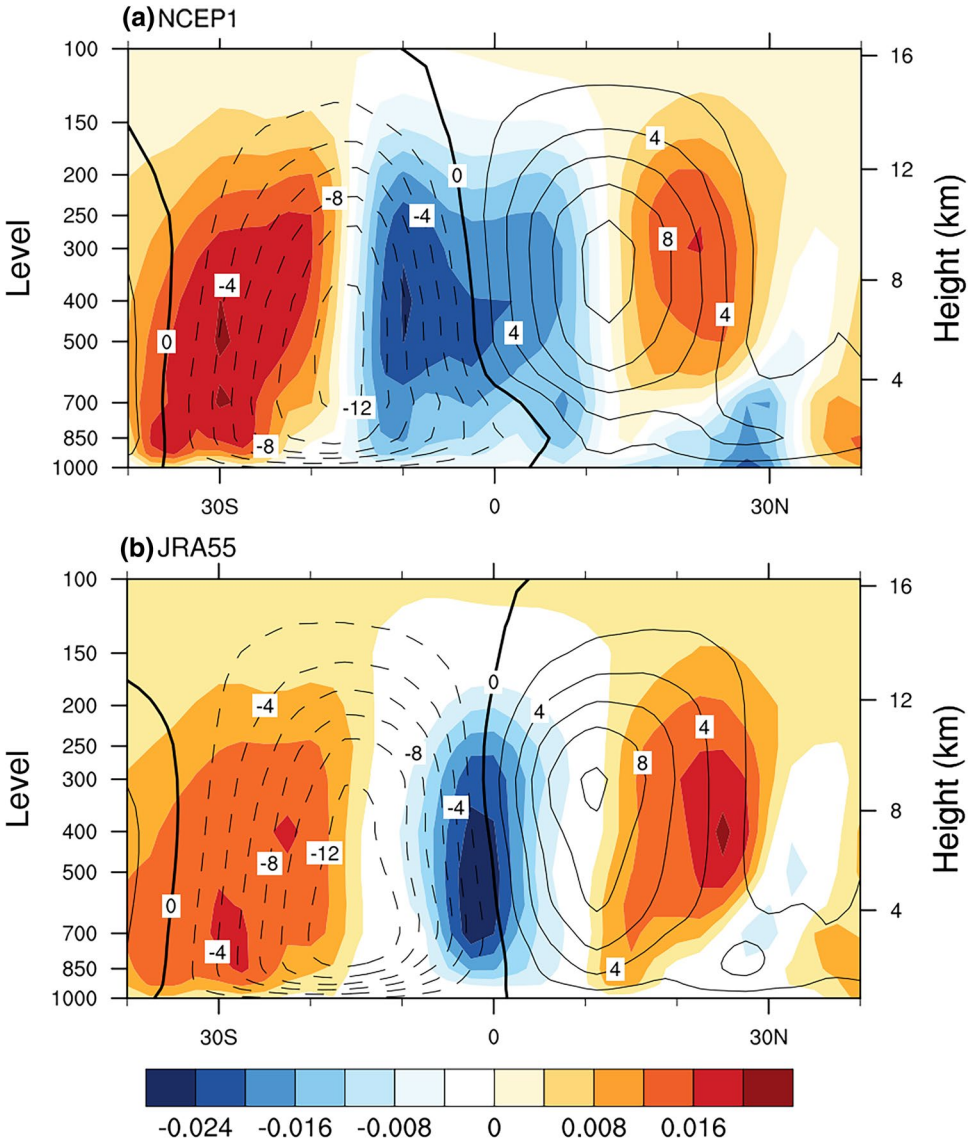

Fig. 1 The spatial distribution of climatological boreal spring regional HC over the Asian monsoon domain based on **a** NCEP/NCAR and **b** JRA55 reanalyses. The contour is the MSF, the dotted line is negative, the solid line is positive, the interval is 0.02×10^{10} kg s^2 and the shading is vertical velocity (unit: m/s)

2.2 Methods

According to the Helmholtz theorem, the horizontal wind field can be decomposed into two parts: the non-divergent part $\boldsymbol{V}_{\psi}$ and the non-rotating part $\boldsymbol{V}_{\chi}$,

$$V = V_{\psi} + V_{\chi} \tag{1}$$

The vertical shear of the non-rotational part of the divergent wind $\boldsymbol{V}_{\chi}$ can be used to describe the horizontal distribution of the tropical meridional and zonal circulation. The latitudinal mean range is 30°–160° E, indicating the Asian monsoon domain.

The regional HC calculation method is obtained by integrating the divergent wind as follows:

$$\psi = \int \frac{2\pi R cos\phi}{g}[\bar{V}_{\chi}]dp, \tag{2}$$

where R is the Earth radius, ϕ is the latitude, g is the gravity acceleration, and p is atmospheric pressure.

Empirical orthogonal function (EOF) decomposition, one of the typical methods of principal component analysis, is being used more often in analyses of spatial-temporal data. EOF is used to extract the dominant modes of variability. Correlation and partial correlation are used to describe the relationship between the regional HC and SST. Effective degrees of freedom are considered in the test (Bretherton et al. 1999). To obtain the effective degree of freedom of the linear trend, the following formulas are used:

$$N^* = \frac{N}{\sum_{\tau=-(N-1)}^{N-1}\left(1-\frac{|\tau|}{T}\right)\rho_{\tau}^2}, \tag{3}$$

N^* is the effective degree of freedom of the sequence, N is the length of the sequence, τ is the lag time length of the sequence autocorrelation, and ρ_{τ} is the autocorrelation coefficient of the sequence lag length of τ.

The formulas for calculating the effective degrees of freedom of the regression, correlation and partial correlation coefficients between two time-series are as follows:

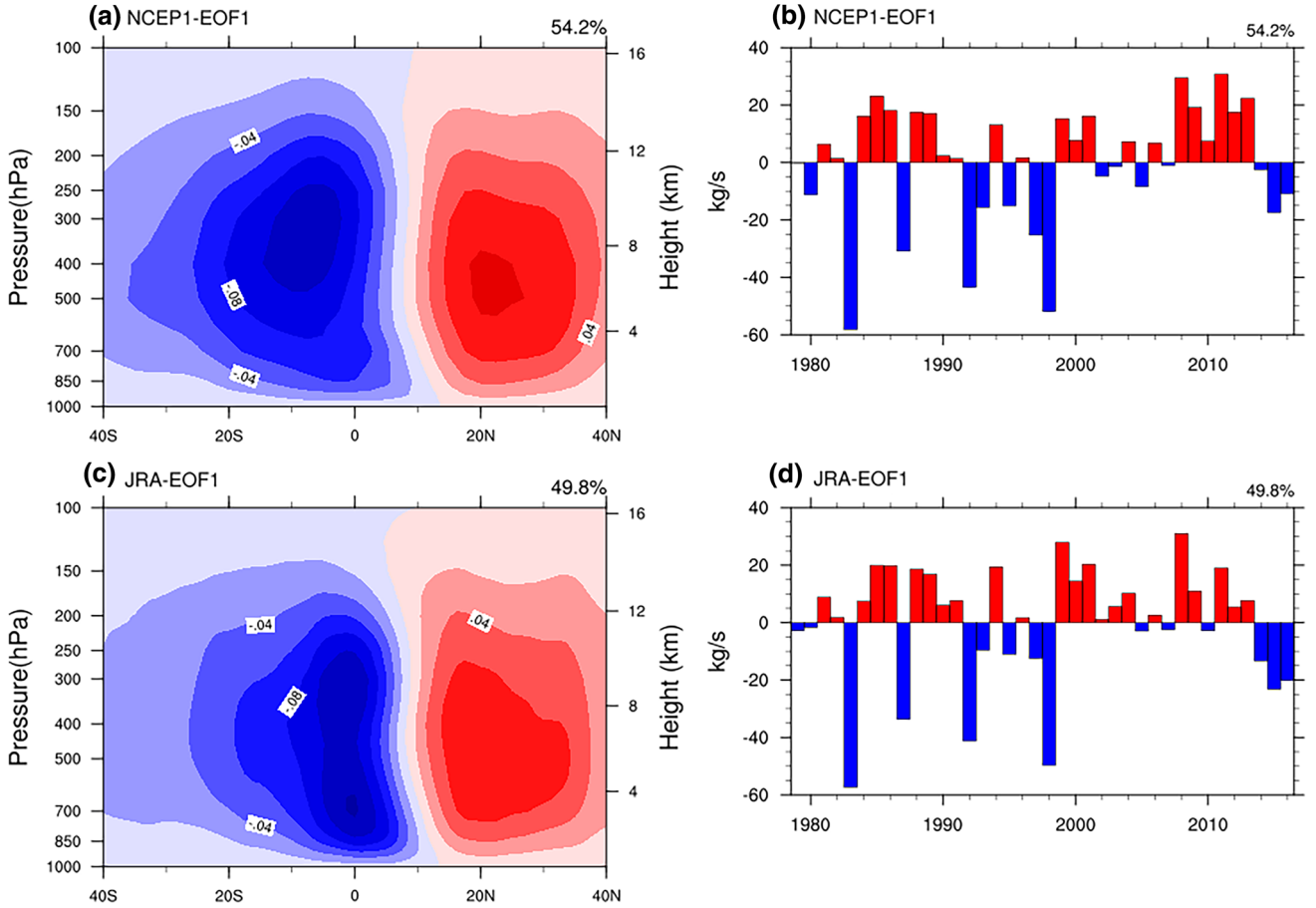

Fig. 2 **a** EOF1 and **b** PC1 of the boreal spring HC over the Asian monsoon domain, based on NCEP/NCAR. **c**, **d** Same as in **a**, **b** but based on the JRA55

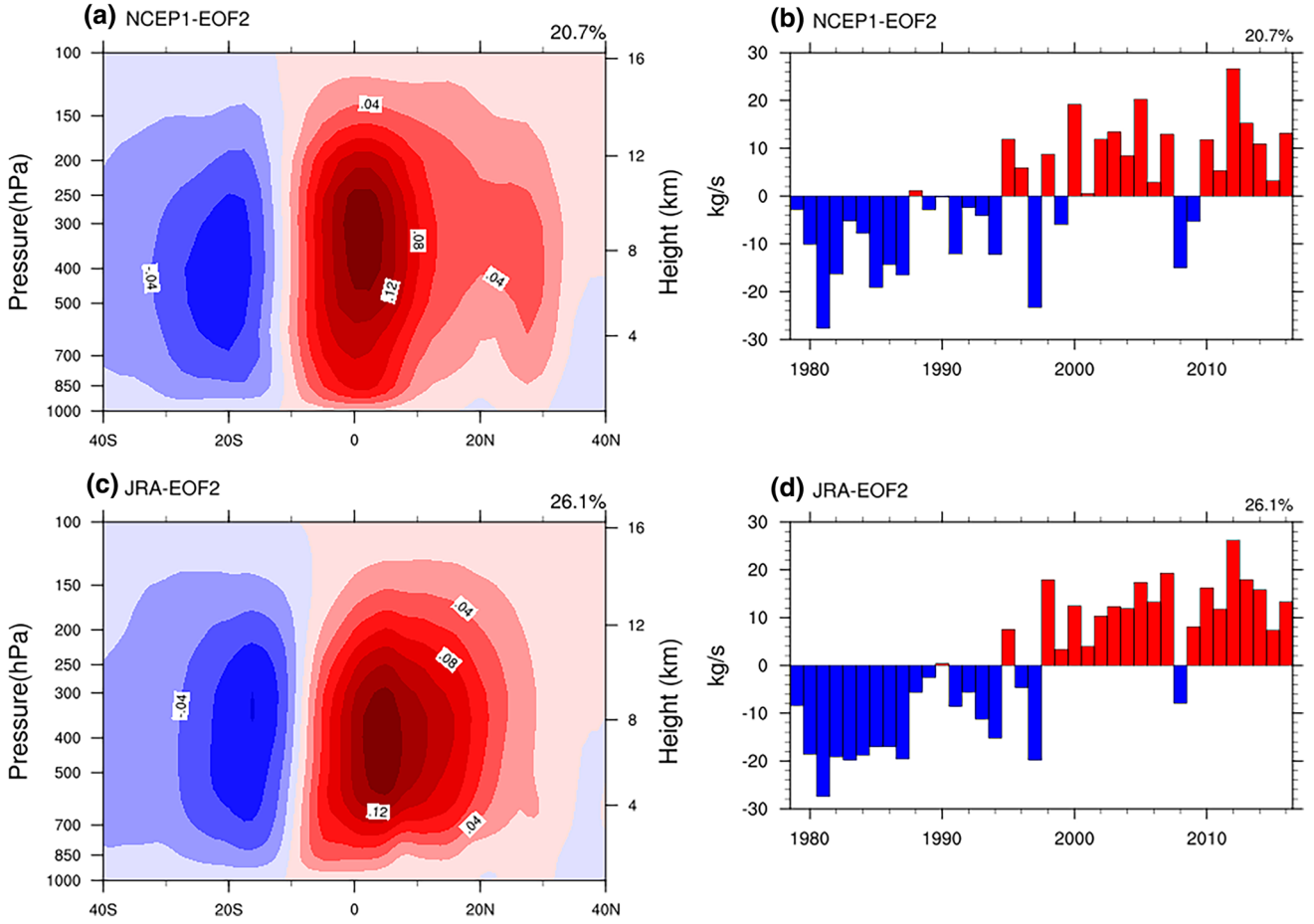

Fig. 3 Same as in Fig. 2, but for EOF2 and PC2

$$N^* = N\frac{1-\rho_1}{1+\rho_1}. \tag{4}$$

2.3 Model

Gill (1980) illustrated a linear shallow-water equation to express the reactions of the tropical and extratropical atmosphere to the heating of an equatorially asymmetric heating source. Recently, some studies were conducted using Gill's model to explore the response of the atmosphere to the thermal force with detailed influences, including the strength, extent of heating and location (Xing et al. 2014; Feng et al. 2016). This model is a practical and simple theoretical model for studying the response of the atmosphere when given a heating source distribution in a specific region (Chao and Wang 1991). The steady-state solution of its one-layer non-dimensional equation is as follows (Ratnam et al. 2012):

$$\varepsilon \mathrm{u} - \frac{1}{2}yu = -\frac{\partial p}{\partial x}, \tag{5}$$

$$\varepsilon v + \frac{1}{2}\mathrm{yu} = -\frac{\partial \mathrm{p}}{\partial \mathrm{y}}, \tag{6}$$

$$\varepsilon p + \frac{\partial u}{\partial x} + \frac{\partial v}{\partial y} = -Q, \tag{7}$$

$$w = \varepsilon p + Q, \tag{8}$$

where x and y represent the distance from the equator to the east and north, ε is a decay factor, u and v are zonal and meridional velocity, respectively, p is pressure disturbances, Q is the heating source, and w is vertical velocity.

3 The variability of the boreal spring HC over the Asian monsoon domain

3.1 Climatological characteristics

The climatological distribution of the boreal spring background averaged during the period of 1979–2016 is first examined. The warmest SST lies in the Asian monsoon

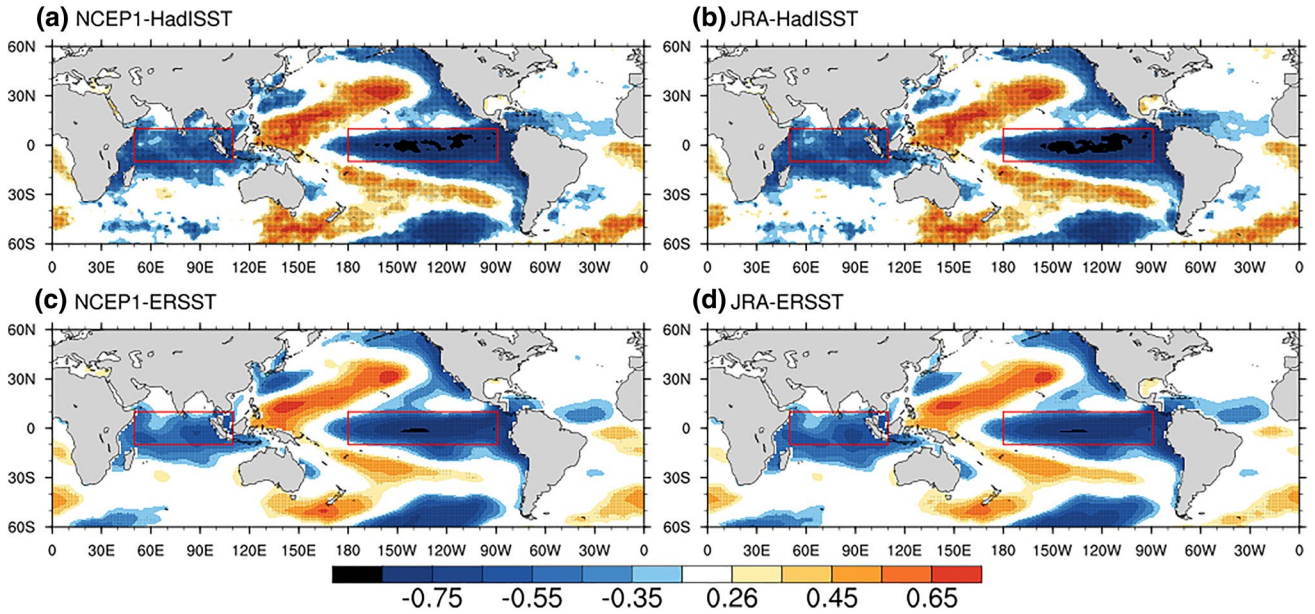

Fig. 4 **a** Spatial distribution of the detrended correlation coefficients between the boreal spring SST and PC1 of the regional HC, based on NCEP/NCAR and HadISST. **b** Same as in (**a**) but based on JRA55 and HadISST. **c** Same as in (**a**) but based on NCEP/NCAR and ERSST. **d** Same as in (**a**) but based on JRA55 and ERSST. Shading indicates significance at the 0.1 level, and dots indicate a valid degree of freedom test. The red boxes are for the tropical eastern Pacific and Indian Ocean discussed in the text

domain, and the maximum center of precipitation is concentrated in this region near the equator (figure not shown). That is, the maximum convective center in boreal spring is located over 10° S–10° N and 50°–150° E, which is included in the Asian monsoon domain. The climatological distribution of boreal spring HC over the Asian monsoon domain, based on the two reanalyses (averaged over 30°–160° E), is shown in Fig. 1. The regional HC is equatorially symmetric, with the ascending branch located around the equator, and the two sinking branches lie at approximately 30° latitude in each hemisphere. The southern cell is slightly stronger than the northern counterpart. The climatological features of the regional HC are consistently observed in the two reanalyses.

3.2 The dominant modes of the regional boreal spring HC

EOF analysis is applied to extract the dominant patterns of boreal spring HC variability over the Asian monsoon domain. Note that only the first two EOF modes are presented as the EOF3 and EOF4 cannot be separated according to *North*'s rule. The spatial and temporal distributions of the first mode (EOF1 and PC1) are shown in Fig. 2. The two datasets show good consistency in both the temporal and spatial distributions. The first mode accounts for approximately 50% of the total variance. PC1 shows a significant long-term upward trend and mainly reflects the interannual variation, which is consistent with the strengthening trend of boreal spring HC over western Pacific as reported (Huang et al. 2019). The spatial distribution is asymmetric about the equator, with the collaborated ascending branch lying at approximately 10° N. The southern cell of this mode extends from 10° N to 30° S, with the main body in the SH centered round 10° S. The northern cell is weaker and located in the NH, centered at approximately 25° N. PC1 shows significant interannual variation, which is consistently observed in the two datasets. In the years of strong El Niño events such as 1983, 1987, 1997, and 1998, PC1 is located in the negative phase, while in the years of La Niña events such as 1984, 1985, 1988, and 2000, the values of PC1 are positive. The linkage between PC1 and ENSO can be verified by the strong correlation between PC1 and the Niño 3 index, with a coefficient of − 0.88; that is, the variation of EOF1 is connected to the ENSO. A similar result is observed based on European Centre for Medium-Range Weather Forecasts (ECMWF) Re-Analysis interim (ERAI; Dee et al 2011), indicating the reliability of the result.

The spatial and temporal distributions of the second mode (EOF2 and PC2), based on the two reanalyses, are shown in Fig. 3. This mode accounts for ~ 20% of the explained variance. Different from the distribution of EOF1, the ascending branch of the EOF2 is located to the south of the equator at approximately 10° S. The two sinking branches lie at approximately 40° S and 30° N, respectively. The northern cell is stronger than the southern cell. Furthermore, PC2

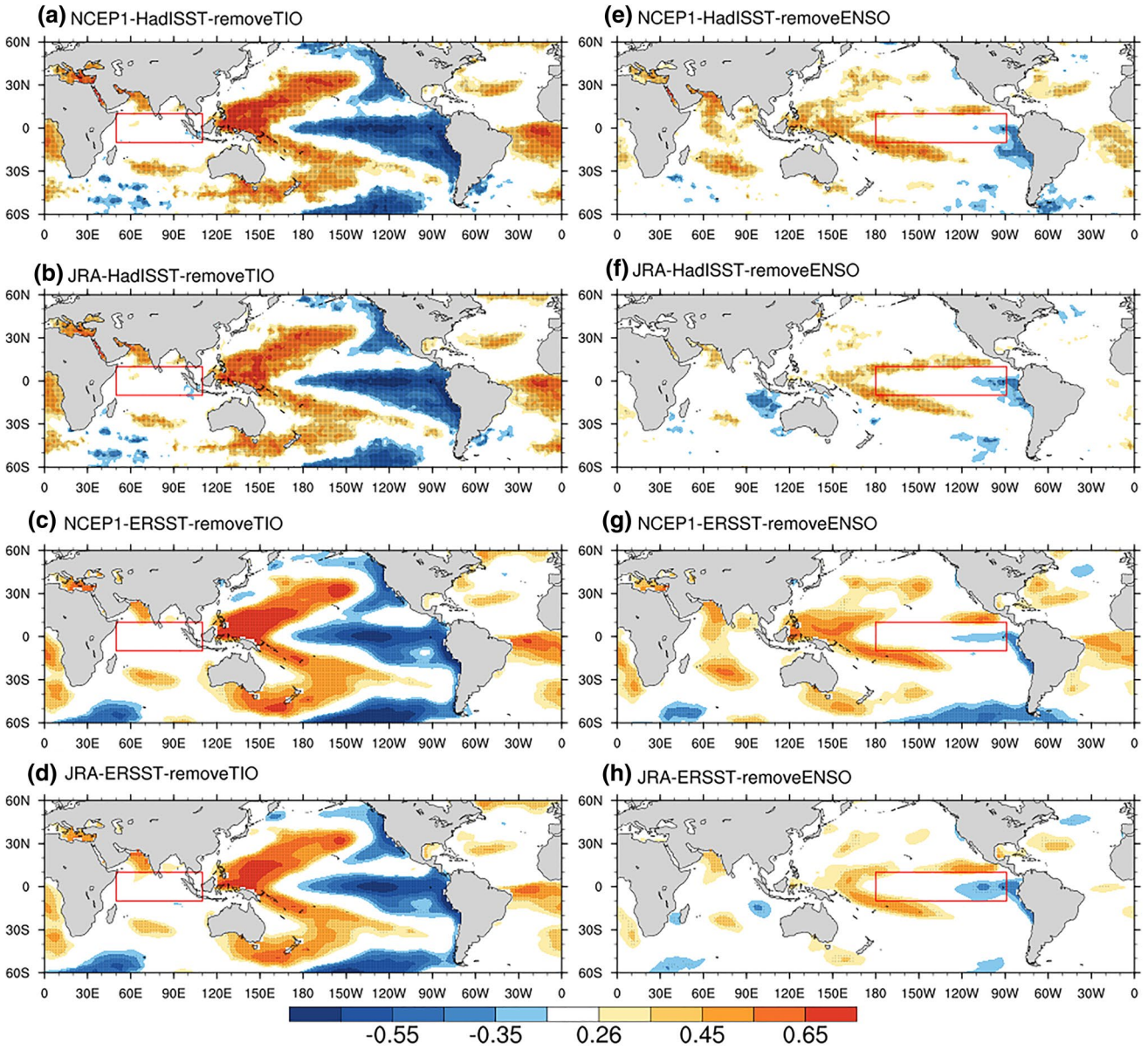

Fig. 5 Left panel: spatial distribution of the correlation coefficients between PC1 of the regional HC and SST after removing the effects of SST averaged over the tropical Indian Ocean based on various datasets. Right panel: same as in the left panel but for the correlations between PC1 of the regional HC and SST after removing the effects of Niño 3 index. Shading indicates significance at the 0.1 level, and dots indicate a valid degree of freedom test. The red boxes are for the tropical eastern Pacific and Indian Ocean discussed in the text

displays an obvious interdecadal variation, being in the negative phase during 1979–1988 and in the positive phase during 1989–2016. That is, PC2 exhibits a significant interdecadal enhanced trend. Notably, the temporal variation of this mode is consistently seen in the two reanalysis datasets, with a correlation coefficient of 0.90, indicating reliability. The above analysis indicates that both the spatial structures and the temporal variations of the first two modes are different. For example, the first mode is dominated by the southern cell, with the ascending branch located north of the equator, showing strong interannual variation. The second mode is dominated by the northern cell, with the rising branch located south of the equator, displaying strong interdecadal variation. This result suggests that the two modes may be affected by different physical factors. The possible influences of the tropical SST on the variation of the modes will be discussed in the following sections.

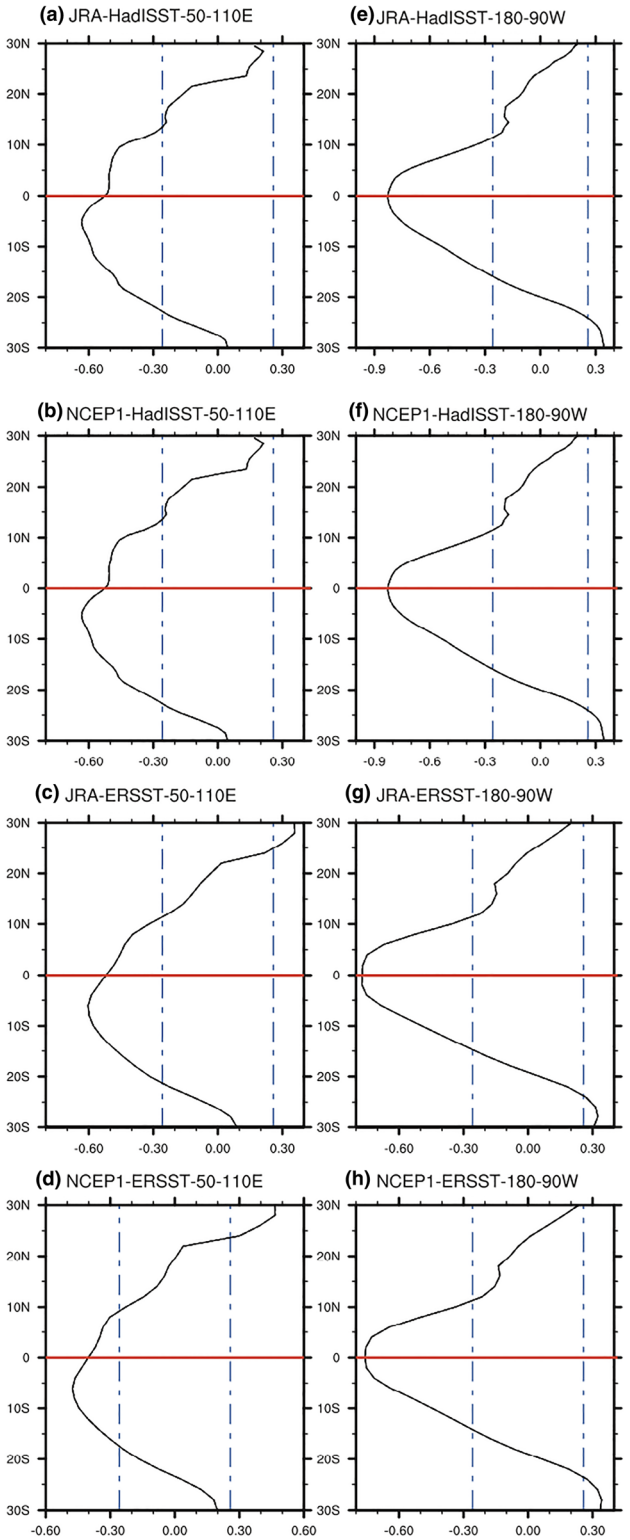

Fig. 6 Left panel: zonal mean correlation coefficients between the PC1 of the regional HC and SST over the tropical Indian Ocean and SST over the based on various datasets. Right panel: same as in the left panel but for the correlation coefficients between the PC1 and eastern Pacific Ocean. Blue dotted lines indicate significance at the 0.1 level, and the red solid line indicates the equator

4 Linkage with the tropical SST

4.1 The linkage between the EOF1 and tropical SST

The correlation between PC1 and SST is shown in Fig. 4. This figure presents a La Niña-like distribution, which is in agreement with various datasets. Significant negative correlations are observed over the TIO and the equatorial eastern Pacific, while significant positive correlations are observed over the tropical western Pacific. This result implies that the variation of SSTs over the TIO and the eastern Pacific may contribute to the variation of EOF1; however, it has been reported that the ENSO has a significant effect on the boreal spring TIO SST (Xie et al. 2009). Negative SST anomalies would be found throughout the entire basin of the TIO during the receding spring of the La Niña event, and vice versa (Chowdary et al. 2006). Here, a partial correlation is employed to distinguish the relative role of the SST over the TIO and eastern Pacific on the variation of EOF1. The variation of SST over the TIO is represented as the areal averaged SST over the region of 50°–110° E, 10° S–10° N, and the Niño 3 index is employed to characterize the variation of ENSO.

The results of partial correlations between the PC1 and SST after removing the effects of SST over the TIO are shown in Fig. 5a–d. A significant negative correlation over the equatorial eastern Pacific is observed, while a significant positive correlation is found in the tropical western Pacific. However, the significant correlations over the TIO are vanished. In the contrary, the correlations between PC1 and SST after removing the effects of the Niño 3 index indicate that significant correlations over 0.70 have largely disappeared (Fig. 5e–h). Moreover, we find that the significant correlation between PC1 and Niño 3 index is maintained when the effect of the TIO SST is removed, changing from −0.88 to −0.72. However, the relationship between PC1 and TIO SST is nonsignificant when the effects of the Niño 3 index are excluded, changing from −0.5 to −0.02. The above results suggest that the significant negative relationship between the TIO SST and PC1 is mainly due to the modulation of ENSO.

The above analysis implies that the variation of EOF1 is related to ENSO. The occurrence of ENSO events would induce significant SST anomalies during boreal spring over the TIO, which in turn would lead to regional HC anomalies. We analyze the zonal mean distribution between the PC1 and SST over the TIO and eastern Pacific, respectively. The correlation coefficient between the PC1 and TIO SST shows an equatorially asymmetric distribution (Fig. 6a–d), with the maximum center of the negative correlation over ~7°S. However, it is equatorially symmetric over the eastern Pacific, with the maximum center around the equator (Fig. 6e, f). According to the results of Feng and Li (2013),

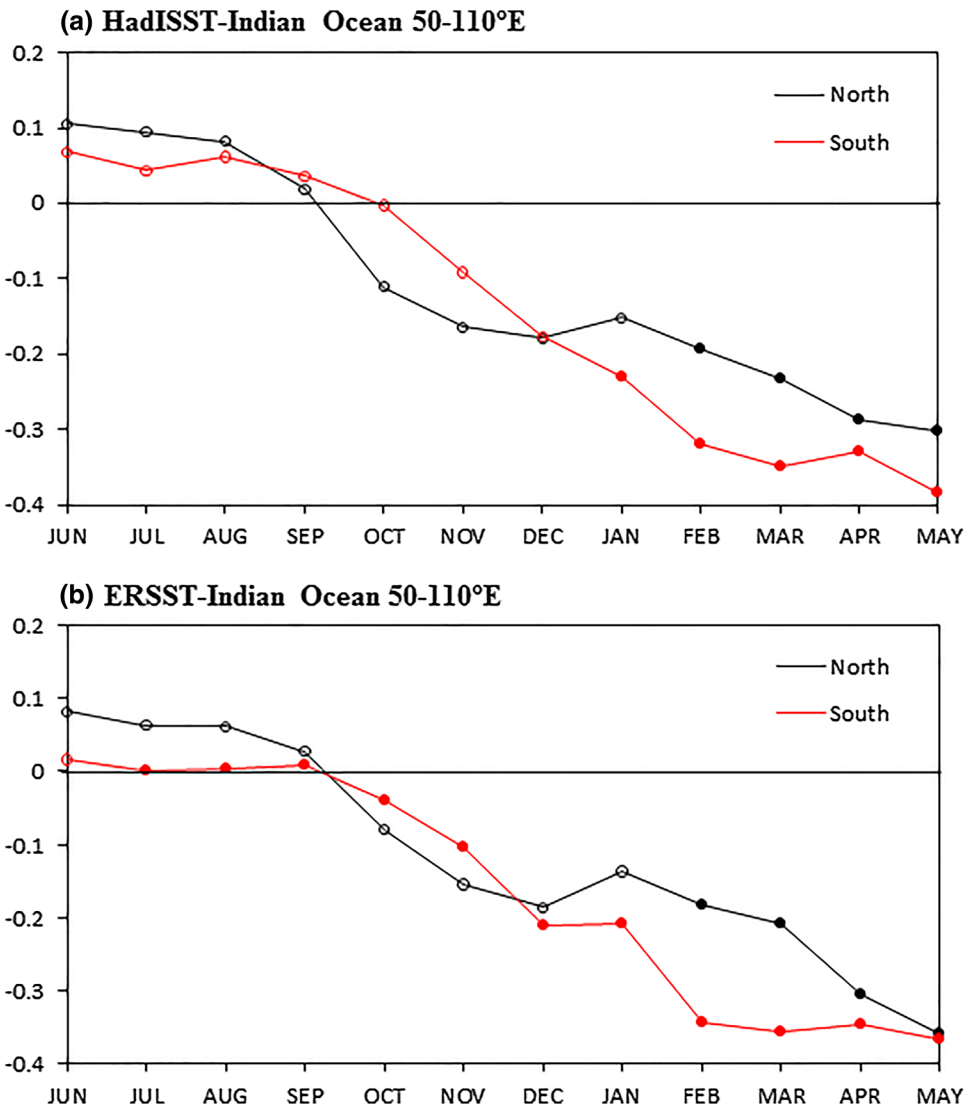

Fig. 7 Areal averaged SST in the southern (10° S–0°, 50°–110° E) and northern (10° S–0°, 50°–110° E) regions of the tropical Indian Ocean during La Niña events based on **a** HadISST and **b** ERSST (solid points are significant at the 0.1 level)

an equatorially symmetric SST anomaly is accompanied with an equatorially symmetric meridional circulation. That is, the distribution of the EOF1 may attach to the TIO SST rather than over the eastern Pacific. This point further verifies the above result. To explore the potential mechanisms of the ascending branch location of the regional HC in the NH, we examine the meridional distribution of SST over the tropical Indian Ocean during the La Niña events (Fig. 7). We see that along with the development of La Niña events, significant cold SST anomalies occur in both the northern (50°–110° E, 0°–10° N) and southern (50°–110° E, 10° S–0°) TIO. However, the SST anomalies over the southern Indian Ocean are greater than those over the northern part during boreal spring. The uneven negative cold SST anomalies over the southern and northern Indian Ocean, accompanied by La Niña events, would induce an anomalous SST meridional gradient. Thus, compared with the southern TIO, the northern counterpart is a warmer heating source, resulting in an anomalous northward meridional SST gradient.

The anomalous ascending of the HC is due to the distribution of the meridional gradient of the tropical SST, i.e., the locations where the meridional gradient of SST is equal to zero are parallel to the position where the anomalous rising occurs (Feng and Li 2013). We further analyzed the meridional gradient of anomalous SST over the TIO during La Niña events (Fig. 8). The location where the meridional gradient of TIO SST (50°–110° E, 10°S–10° N) equals zero lies to the north of the equator in both the ERSST and HadISST. Therefore, an anomalous equatorially asymmetric

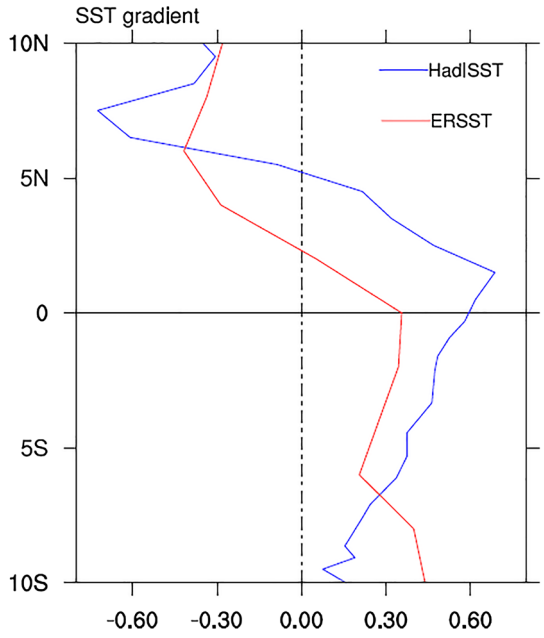

Fig. 8 Meridional gradient of zonal mean SST anomalies averaged over the tropical Indian Ocean SST (50°–110° E) during La Niña events based on the ERSST (red) and HadISST (blue) datasets

meridional circulation with an ascending branch north of the equator would be induced under the influence of anomalous TIO SST along with La Nina events.

4.2 The linkage between the EOF2 and tropical SST

The correlation between PC2 and SST is shown in Fig. 9. Significant positive correlations can be seen over the Asian monsoon domain and tropical Atlantic Ocean. These significant correlations are consistently observed across the various datasets. Considering that PC2 exhibits strong interdecadal intensification, a detrended correlation between PC2 and SST is performed. The significant positive correlations nearly disappeared (Fig. 9e–h) when the linear trend is removed. This result indicates that the enhancement in PC2 is due to warming of the tropical SST. This conclusion is further verified by the significant correlation between the PC2 and the areal mean TIO SST (as in Fig. 8), with a coefficient of 0.58; however, the correlation decreases to 0.09 when the linear trend is removed. The above result indicates that the temporal variation of EOF2 is related to the warming trend of the SST over the Asian monsoon domain. However, the reason that the ascending branch of EOF2 is located to the south of the equator is still unknown. To answer this question, we further analyzed the long-term trend of regional average SST in the two regions, i.e., south of the equator and north of the equator within the Asian monsoon domain.

We analyze the interdecadal variation of regional averaged SST over 10° S–0° and 0°–10° N within 30°–160° E to examine the warming rate in the southern and northern scope of the Asian monsoon domain. Figure 10 displays the variation of SSTs averaged over the northern and southern scopes of the Asian monsoon domain, as well as their linear trends, and we find that the SST over the two regions both present a significant warming trend. However, the warming rate in the southern region is more rapid than that in the northern region. The rapid warming rate in the southern Indian Ocean is consistently observed in the two SST datasets. Therefore, the spatial distribution of the EOF2 is due to the uneven warming rate of the SST in the southern and northern Indian Ocean, resulting in the migration of the rising branch of the regional HC to the south of the equator.

5 Verification of Gill's model

To verify the above conclusion, we forced a weak heating source near 10 °N and 100 °E in *Gill*'s model, as shown in Fig. 11a. The central intensity of the heat source is 0.2 °C, corresponding to the anomalous amplitude during the La Niña events, i.e., the SST over the northern TIO is warmer than that over the southern. The intensity of the heating source decreases from the center to all sides. The formula of the heat source in Gill's model is as follows:

$$Qx, y = A \cdot g(x) \cdot e^{-\frac{1}{4}(y+d)^2},$$

$$g(x) = \begin{cases} \cos kx, & |x| \le L \\ 0, & |x| > L \end{cases}, k = \pi/2L. \tag{9}$$

Among the coefficients, Q represents the heat source, A represents the heat source intensity, d is the longitudinal distance from the equator to the heat source center, $d>0$ ($d<0$) represents the latitudinal width of the heat source center in the SH (NH), and 2L represents the latitudinal width of the heat source. The atmospheric circulation stimulated by the heat sources is shown in Fig. 11b. When the heating source lies at 10° N, the ascending branch of the HC forced by the heat source is also located near 10° N. That is, the SST in the NH is slightly warmer than in the SH during the La Niña years, which leads to an ascending branch of regional HC located to the north of the equator. These model results further support the observed result.

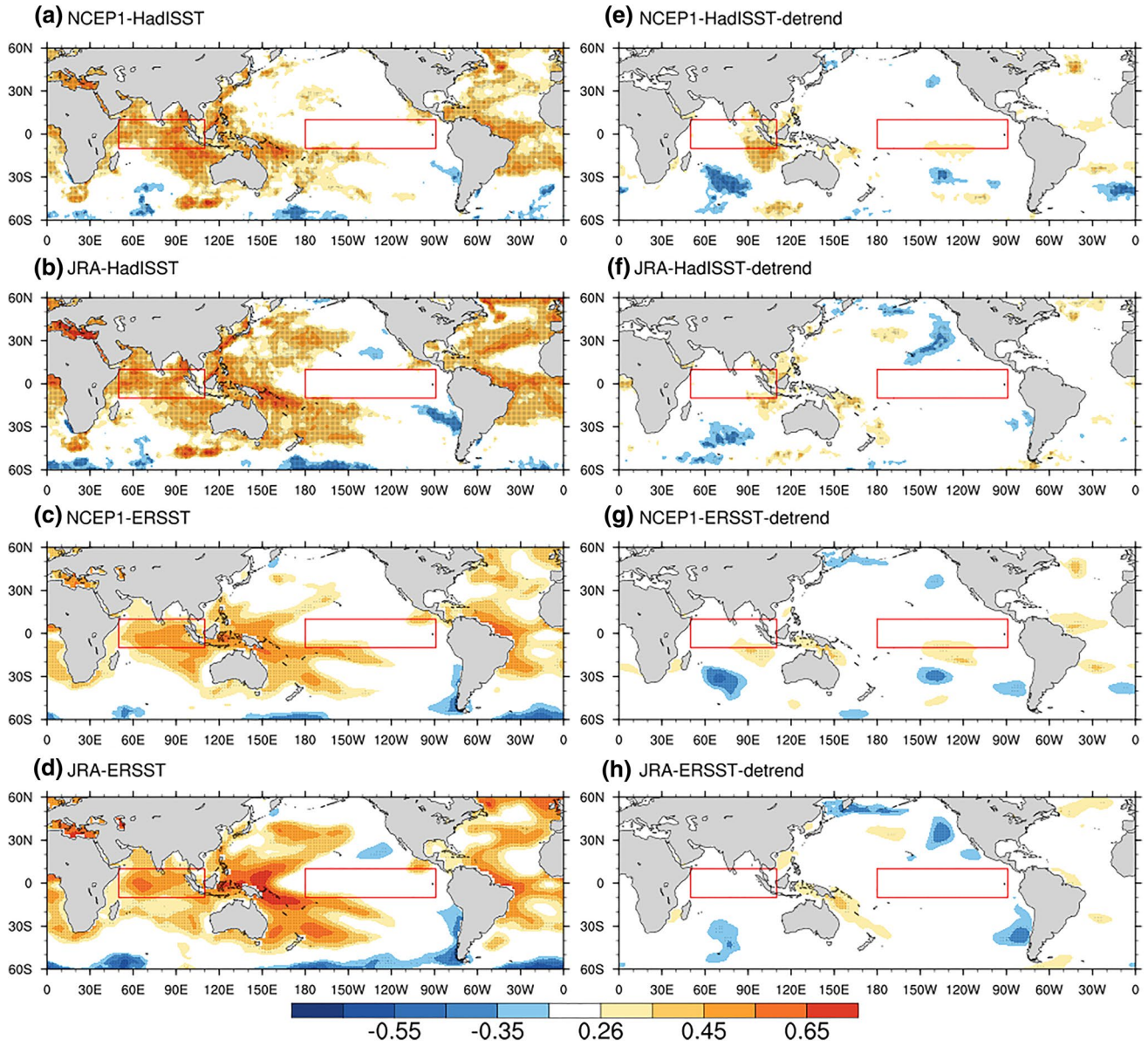

Fig. 9 Left panel: spatial distribution of the correlation coefficients between PC2 of the regional HC and SST based on various datasets. Right panel: same as in the left panel but for the detrended correlations. Shading indicates significance at the 0.1 level, and dots indicate a valid degree of freedom test. The red boxes are for the tropical eastern Pacific and Indian Ocean discussed in the text

6 Summary and discussion

The variability of boreal spring HC in the Asian monsoon domain is studied using a 38-year dataset from 1979 to 2016. The characteristics of the temporal and spatial variations of the regional HC are described. The first dominant mode of the regional HC is dominated by the southern cell, with the ascending branch lying to the north of the equator. The variation of this mode is connected to the ENSO. Along with the development of La Niña events, significant negative SST anomalies occur over the TIO. In addition, the magnitude of the negative SST anomalies in the southern TIO is greater than that in the northern counterpart. Thus, an anomalous SST meridional gradient is induced and pointed to the northern TIO, resulting in an anomalous regional HC that ascends north of the equator. The second dominant mode of the regional HC is dominated by interdecadal variability, showing an evident

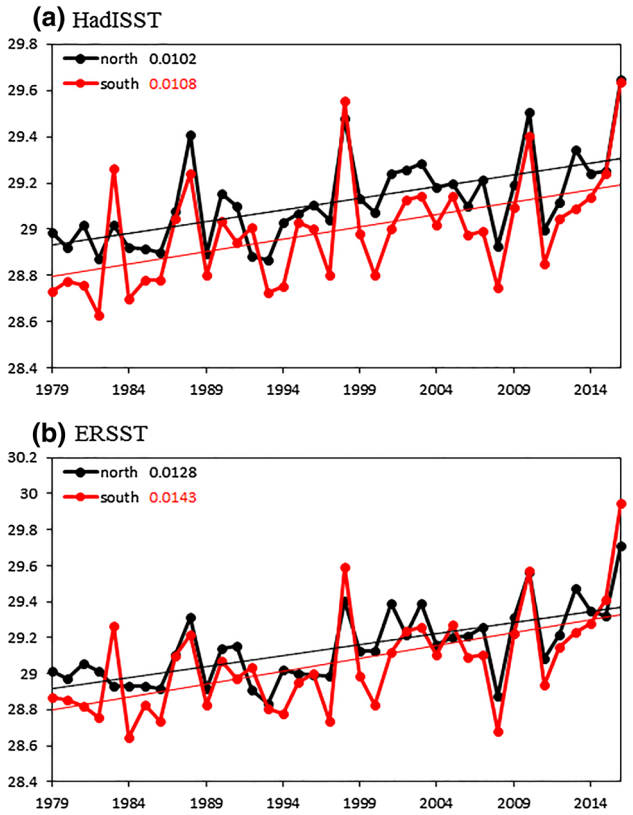

Fig. 10 Time series of the areal mean SST over the southern (10° S–0°) and northern (0°–10° N) tropical Indian Ocean, as well as their linear trends based on **a** HadISST and **b** ERSST

enhancement in recent decades. The ascending branch of the EOF2 is located to the south of the equator. The temporal variation of EOF2 is related to the uneven warming of SST over the Asian monsoon domain. The ascending branch of EOF2 lies at south of the equator because the warming rate of the SST over the Asian monsoon domain is inhomogeneous, with a more rapid rate in the southern counterpart.

In addition, the La Niña events are connected with an anomalous HC, with distinct south wind anomalies in the low troposphere, which is the same as the prevailing wind of the Asian summer monsoon. This finding suggests that the occurrence of a La Niña event is favorable for a strong monsoon circulation and is consistent with previous results. For example, it is reported that a significant correlation is found between the Indian monsoon rainfall and the equatorial Indian Ocean wind during the El Niño period (Chie et al. 2008). When a La Niña event occurs, the Indian summer monsoon and rainfall increase. Webster and Yang (1992) also noted that the variation of Asian monsoons is related to ENSO. El Niño is usually associated with weaker monsoons, while La Niña is associated with stronger monsoons. Since the 1970s, the East Asian monsoon and the East South Asian monsoon circulation have both weakened to varying degrees (Wang 2001a; Chase et al. 2003; Zhou 2008). The frequency of La Niña incidents has also decreased since the 1970s (Hoell et al. 2014), favoring the formation of a weak monsoon.

On the other hand, the extratropical atmospheric variability, such as the North Atlantic Oscillation (NAO), shows significant influences on ENSO (e.g., Nakamura et al. 2006; Chen et al. 2014b). We found that the variation of regional HC is closely linked with the ENSO and thus whether the extratropical signals plays a role in affecting the regional HC. Further work regarding this aspect would improve the understanding of the tropical-extratropical interactions and would be helpful for a better recognition of the variability of the regional HC. Meanwhile, because the ascent and descent of the HC is closely connected to convection and rainfall, we find that the variation in the EOF1 is accompanied by a dipole anomaly in the convection within the TIO (figure not shown). That is, the regional HC may play a certain role in impacting rainfall variation, and future work will further investigate the influence of variability of the regional HC on the regional climate.

Finally, during La Niña events, the SST in the southern TIO was colder than that in the northern. Most previous studies have mainly considered latitudinal variations in SST or have considered the Indian Ocean as a whole (Santoso et al. 2015; Xie et al. 2009). The meridional structure of the Indian Ocean SST is less discussed. Therefore, it is essential to further study the possible reason for this uneven cooling, to compare whether there are similar cooling differences in the two types of ENSO events and to study the related climate effects, especially the impact on regional climate. Furthermore, the air-sea system showed strong interdecadal variability in the late 1970s (Wang et al. 2008). It is necessary to study whether this interdecadal variation will affect the meridional structure of SST as well as the response of the atmosphere to the anomalous SST meridional structure.

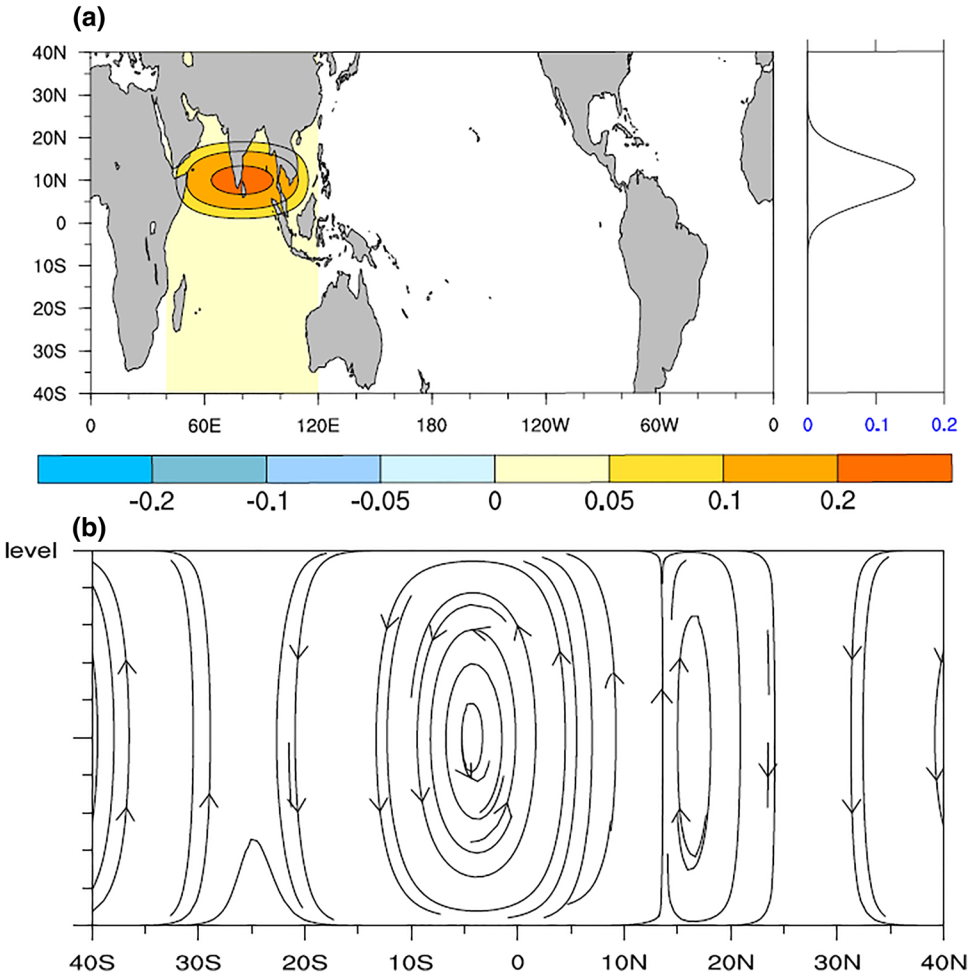

Fig. 11 **a** Distribution of the anomalous heating distribution in the theoretical experiment. **b** Corresponding meridional circulation under the influence of heating

Acknowledgements This work was jointly supported by the National Key R&D Program of China (2016YFA0601801), National Natural Science Foundation of China (NSFC) Project (41975079), and the SOA Program on Global Change and Air-Sea interactions (GASI-IPOVAI-03). The HadISST dataset was obtained from the UK Met Office Hadley Centre and is available online at http://www.metoffice.gov.uk/hadobs/hadisst/data/download.html. The NCEP1 and ERSST reanalyses were obtained from NOAA and are available at http://www.esrl.noaa.gov/psd/data/gridded/. The JRA reanalysis is available online at http://jra.kishou.go.jp/JRA-55/index_en.html.

References

Bretherton CS, Widmann M, Dymnikov VP, Wallace JM, Bladé L (1999) The effective number of spatial degrees of freedom of a time-varying field. J Climate 12:1990–2009. https://doi.org/10.1175/1520-0442(1999)012%3c1990:TENOSD%3e2.0.CO;2

Chao JP, Wang ZG (1991) Influence of the ocean heating scale on the structure of the vertical circulation cell in the tropical atmosphere. J Nanjing Inst Meteorol 14:10–17

Chase TN, Knaff JA, Pielke RA, Kalnay E (2003) Changes in global monsoon circulations since 1950. Nat Hazards 29:229–254. https://doi.org/10.1023/a:1023638030885

Chen SF, Wei K, Chen W, Song LY (2014a) Regional changes in the annual mean Hadley circulation in recent decades. J Geophys Res Atmos 119(13):7815–7832. https://doi.org/10.1002/2014JD021540

Chen SF, Yu B, Chen W (2014b) An analysis on the physical process of the influence of AO on ENSO. Climate Dyn 42(3–4):973–989

Chen L, Yu YQ, Zheng WP (2016) Improved ENSO simulation from climate system model FGOALS-g1.0 to FGOALS-g2. Climate Dyn 47:2617–2634. https://doi.org/10.1007/s00382-016-2988-8

Chen L, Li T, Yu YQ, Behera SK (2017) A possible explanation for the divergent projection of ENSO amplitude change under global warming. Climate Dyn 49:3799–3811. https://doi.org/10.1007/s00382-017-3544-x

Chie I, Kushnir Y, Mark AC, Kaplan A (2008) Timing of El Niño-related warming and Indian summer monsoon rainfall. J Climate 21(11):2711–2719. https://doi.org/10.1175/2007JCLI1979.1

Chowdary JS, Gnanaseelan C, Vaid BH, Salvekar PS (2006) Changing trends in the Tropical Indian Ocean SST during the La Niña years. Geophys Res Lett 33:L18610. https://doi.org/10.1029/2006GL026707

Dai AG (2013) Increasing drought under global warming in observations and models. Nat Climate Change 3:52–58. https://doi.org/10.1038/nclimate1811

Dee DP, Uppala SM, Simmons AJ et al (2011) The ERA-Interim reanalysis: configuration and performance of the data assimilation system. Q J R Meteorol Soc 137(656):553–597. https://doi.org/10.1002/qj.828

Feng J, Li JP (2013) Contrasting impacts of two types of ENSO on the boreal spring Hadley circulation. J Climate 26:4773–4789. https://doi.org/10.1175/JCLI-D-12-00298.1

Feng J, Li JP, Jin FF, Liu ZY, Xing N, Guo YP (2016) Contrasting responses of the hadley circulation to equatorially asymmetric and symmetric meridional sea surface temperature structures. J Climate 29:8949–8963. https://doi.org/10.1175/JCLI-D-16-0171.1

Feng J, Li JP, Jin FF, Liu ZY, Zhao S (2019) Effect of El Niño on the response ratio of Hadley circulation to different SST meridional structures. Climate Dyn. https://doi.org/10.1007/s00382-019-04756-7

Freitas AV, Ambrizzi T (2015) Recent changes in the annual mean regional Hadley circulation and their impacts on South America. Adv Meteorol. https://doi.org/10.1155/2015/780205

Freitas AV, Aímola L, Ambrizzi T, Oliveira CP (2017) Changes in intensity of the regional Hadley cell in Indian ocean and its impacts on surrounding regions. Meteorol Atmos Phys 129(3):229–246. https://doi.org/10.1007/s00703-016-0477-6

Fu Q, Johanson CM, Wallace JM, Reichler T (2006) Enhanced mid-latitude tropospheric warming in satellite measurements. Science 312:1179. https://science.sciencemag.org/content/312/5777/1179

Fyfe JC, Gillett NP, Marshall GJ (2012) Human influence on extratropical Southern Hemisphere summer precipitation. Geophys Res Lett 39:L23711. https://doi.org/10.1029/2012GL054199

Gill AE (1980) Some simple solutions for heat-induced tropical circulation. Quart J Roy Meteor Soc 106(449):447–462

Guo YP, Tan ZM (2018) Impacts of the boreal spring Indo-Pacific warm pool Hadley circulation on tropical cyclone activity over the western North Pacific. J Climate 31:1361–1375. https://doi.org/10.1175/JCLI-D-17-0422.1

Guo YP, Li JP, Feng J, Xie F, Sun C, Zheng JY (2016) The multidecadal variability of the asymmetric mode of the boreal autumn Hadley circulation and its link to the Atlantic Multidecadal Oscillation. J Climate 29:5625–5641. https://doi.org/10.1175/jcli-d-15-0025.1

Hadley G (1735) Concerning the cause of the general trade-winds: By Geo. Hadley, Esq; FRS. Philos Trans 39(436–444):58–62

Hoell A, Funk C, Barlow M (2014) La Niña diversity and northwest Indian Ocean rim teleconnections. Climate Dyn 43:2707–2724. https://doi.org/10.1007/s00382-014-2083-y

Hou AY (1998) Hadley circulation as a modulator of the extratropical climate. J Atmos Sci 55:2437–2457. https://doi.org/10.1175/1520-0469(1998)055%3c2437:HCAAMO%3e2.0.CO;2

Hou AY, Lindzen RS (1992) The influence of concentrated heating on the Hadley circulation. J Atmos Sci 49(14):1233–1241. https://doi.org/10.1175/1520-0469(1992)049%3c1233:TIOCHO%3e2.0.CO;2

Huang RP, Chen SF, Chen W, Hu P (2018a) Has the regional Hadley circulation over western Pacific during boreal winter been strengthening in recent decades? Atmos Ocean Sci Lett 11(454–463):362

Huang RP, Chen SF, Chen W, Hu P (2018b) Interannual variability of regional Hadley circulation intensity over western Pacific during boreal winter and its climatic impact over Asia-Australia region. J Geophys Res Atmos 123:344–366. https://doi.org/10.1002/2017JD027919

Huang RP, Chen SF, Chen W, Hu P, Yu B (2019) Recent strengthening of the regional Hadley circulation over the western Pacific during boreal spring. Adv Atmos Sci. https://doi.org/10.1007/s00376-019-9004-2

Kalnay E, Kanamitsu M, Kistler R, Collins W, Deaven D, Gandin L (1996) The NCEP/NCAR 40-year reanalysis project. Bull Am Meteorol Soc 77(3):437–472. https://doi.org/10.1175/1520-0477(1996)077%3c0437:TNYRP%3e2.0.CO;2

Kobayashi S et al (2015) The JRA-55 reanalysis: general specifications and basic characteristics. J Meteorol Soc Japan 93:5–48. https://doi.org/10.2151/jmsj.2015-001

Li CF, Michio YA (1996) The onset and interannual variability of the Asian Summer Monsoon in relation to land-sea thermal contrast. J Climate 9:358–375. https://doi.org/10.1175/1520-0442(1996)009%3c0358:TOAIVO%3e2.0.CO;2

Mitas C, Clement A (2006) Recent behaviour of Hadley cell and tropical thermodynamics in climate models and re-analyses. Geophys Res Lett 33:L01810. https://doi.org/10.1029/2005GL024406

Nakamura T, Tachibana Y, Honda M, Yamane S (2006) Influence of the Northern Hemisphere annular mode on ENSO by modulating westerly wind bursts. Geophys Res Lett 33(7):L07709

Nguyen H, Evans A, Lucas C, Smith I, Timbal B (2013) The Hadley circulation in reanalyses: climatology, variability, and change. J Climate 26:3357–3376. https://doi.org/10.1175/JCLI-D-12-00224.1

Nguyen H, Lucas C, Evans A, Timbal B, Hanson L (2015) Expansion of the Southern Hemisphere Hadley cell in response to greenhouse gas forcing. J Climate 28(20):8067–8077. https://doi.org/10.1175/JCLI-D-15-0139

Nguyen H, Hendon HH, Lim EP, Boschat G, Maloney E, Timbal B (2017) Variability of the extent of the Hadley circulation in the southern hemisphere: a regional perspective. Climate Dyn 21:1–14. https://doi.org/10.1007/s00382-017-3592-2

Numaguti A (1995) Dynamics and energy balance of the Hadley circulation and the tropical precipitation zones. Part II: sensitivity to meridional SST distribution. J Atmos Sci 52(8):1128–1141. https://doi.org/10.1175/1520-0469(1995)052%3c1128:DAEBOT%3e2.0.CO;2

Oort AH, Yienger JJ (1996) Observed interannual variability in the Hadley circulation and its connection to ENSO. J Climate 9(11):2751–2767. https://doi.org/10.1175/1520-0469(1995)052%3C1128:DAEBOT%3E2.0.CO;2

Quan XW, Diaz HF, Hoerling MP (2004) Change in the tropical Hadley cell since 1950. The Hadley circulation: past, present, and future. Cambridge University Press, Cambridge, pp 85–120

Ratnam JV, Behera SK, Masumoto Y, Takahashi K, Yamagata T (2012) Anomalous climatic conditions associated with the El Niño Modoki during boreal winter of 2009. Climate Dyn 39:227–238. https://doi.org/10.1007/s00382-011-1108-z

Rayner NA, Parker DE, Horton EB, Folland CK, Alexander LV, Rowell DP, Kent EC, Kaplan A (2003) Global analyses of sea surface temperature, sea ice and night marine air temperature since the late nineteenth century. J Geophys Res 108:4407. https://doi.org/10.1029/2002JD002670

RenéD G, Patricio A (2001) Interannual Rainfall Variability over the South American Altiplano. J Climate 14:2779–2789. https://doi.org/10.1175/1520-0442(2001)014%3c2779:IRVOTS%3e2.0.CO;2

Rind D, Rossow WB (1984) The effects of physical processes on the Hadley circulation. J Atmos Sci 41(4):479–507. https://doi.org/10.1175/1520-0469(1984)041%3c0479:teoppo%3e2.0.CO;2

Santoso A, England MH, Cai W (2015) Impact of Indo-Pacific feedback interactions on ENSO dynamics diagnosed using ensemble climate simulations. J Climate 28(13):5017–5029. https://doi.org/10.1175/JCLI-D-14-00114.1

Schneider EK, Lindzen RS (1977) Axially symmetric steady-state models of the basic state for instability and climate studies. Part I. Linearized calculations. J Atmos Sci 34(2):263–279. https://doi.org/10.1175/1520-0469(1977)034%3c0263:asssmo%3e2.0.co;2

Schott FA, Xie SP, McCreary JP (2008) Indian Ocean circulation and climate variability. Rev Geophys. https://doi.org/10.1029/2007RG000245 **(In press)**

Seager R, Harnik N, Kushnir Y, Robinson W, Miller J (2003) Mechanisms of hemispherically symmetric climate variability. J Climate 16:2960–2978. https://doi.org/10.1175/1520-0442(2003)016%3c2960:MOHSCV%3e2.0.CO;2

Smith TM, Reynolds RW, Peterson TC, Lawrimore J (2008) Improvements to NOAA's historical merged land–ocean surface temperature analysis (1880–2006). J Climate 21:2283–2296. https://doi.org/10.1175/2007JCLI2100.1

Stachnik JP, Schumacher C (2011) A comparison of the Hadley circulation in modern reanalyses. J Geophys Res Atmos 116:D22102. https://doi.org/10.1029/2011JD016677

Sun Y, Zhou T (2014) How does El Niño affect the interannual variability of the boreal summer Hadley circulation? J Climate 27:2622–2642

Trenberth KE, Stepaniak DP (2003) Seamless poleward atmospheric energy transports and implications for the Hadley circulation. J Climate 16(22):3706–3722. https://doi.org/10.1175/1520-0442(2003)016%3c3706:spaeta%3e2.0.co;2

Wang B (2001a) Interannual variability of the Asian Summer Monsoon: contrasts between the Indian and the Western North Pacific-East Asian Monsoons. J Climate 14:4073–4090. https://doi.org/10.1175/1520-0442(2001)014%3c4073:ivotas%3e2.0.co;2

Wang HJ (2001b) The weakening of the Asian monsoon circulation after the end of 1970's. Adv Atmos Sci 18:376–386. https://doi.org/10.1007/BF02919316

Wang CZ (2002) Atmospheric circulation cells associated with the El Niño-Southern oscillation. J Climate 15(4):399–419. https://doi.org/10.1175/1520-0442(2002)015%3c0399:ACCAWT%3e2.0.CO;2

Wang C (2004) ENSO, Atlantic climate variability, and the Walker and Hadley circulations. In: Diaz HF, Bradley RS (eds) The Hadley circulation: present, past and future. Advances in global change research, vol 21. Kluwer Academic, New York, pp 173–202

Wang C (2005) ENSO, Atlantic climate variability, and the Walker and Hadley circulations. In: Diaz HF, Bradley RS (eds) The Hadley circulation: present, past, and future. Kluwer Acad, New York, pp 173–202

Wang B, Yang J, Zhou TJ, Wang B (2008) Interdecadal changes in the major modes of Asian-Australian Monsoon variability: strengthening relationship with ENSO since the Late 1970s. J Climate 21(8):1771–1789. https://doi.org/10.1175/2007JCLI1981.1

Webster PJ, Yang S (1992) Monsoon and ENSO: selectively interactive systems. Q J R Meteorol Soc 118:877–926. https://doi.org/10.1002/qj.49711850705

Xie SP, Hu K, Hafner J, Tokinaga H, Du Y, Huang G, Sampe T (2009) Indian Ocean capacitor effect on Indo-Western Pacific climate during the summer following El Niño. J Climate 22(3):730–747. https://doi.org/10.1175/2008JCLI2544.1

Xing N, Li JP, Li YK (2014) Response of the tropical atmosphere to isolated equatorial asymmetric heating (in Chinese). Chin J Atmos Sci 38:1147–1158

Zeng G, Wang WC, Sun ZB, Li ZX (2011) Atmospheric circulation cells associated with anomalous East Asian winter monsoon. Adv Atmos Sci 28(4):913–926. https://doi.org/10.1007/s00376-010-0100-6

Zhang G, Wang Z (2013) Interannual variability of the Atlantic Hadley circulation in boreal summer and its impacts on tropical cyclone activity. J Climate 26(21):8529–8544. https://doi.org/10.1175/JCLI-D-12-00802.1

Zhang WJ, Wang L, Xiang BQ, Qi L, He JH (2015) Impacts of two types of La Niña on the NAO during boreal winter. Climate Dyn 44:1351–1366. https://doi.org/10.1007/s00382-014-2155-z

Zhou, TJ, Yu RC, Li HM, Wang B (2008) Ocean forcing to changes in global monsoon precipitation over the recent half-century. J Climate 21:3833–3852. https://journals.ametsoc.org/doi/pdf/10.1175/2008JCLI2067.1